Machine Learning with Applications 7 (2022) 100216

Contents lists available at ScienceDirect

Machine Learning with Applications

journal homepage: www.elsevier.com/locate/mlwa

A machine learning framework for guided wave-based damage detection of rail head using surface-bonded piezo-electric wafer transducers

Harsh Mahajan, Sauvik Banerjee *

Department of Civil Engineering, Indian Institute of Technology Bombay, Powai, Mumbai 400 076, India

ARTICLE INFO

Keywords:
Rail inspection
Guided wave
Surface bonded sensors
Rail head damage detection
Machine learning application

ABSTRACT

Due to repeated heavy loads, environmental conditions and non-frequent monitoring, the rail is subjected to heavy damage resulting in sudden failure. Hence, a frequent, faster, and efficient monitoring strategy is required. This paper attempts to investigate the application of guided wave (GW) generated through surface-bonded piezo-electric wafer transducer (PWT) to detect damages in rail at high frequencies. Firstly, a combined experimental and simulation study is presented in an effort to understand the dispersion characteristics of guided wave and its interaction with head damages in a relatively small rail specimen. The numerical simulation results are validated with those obtained from the experiments showing a good agreement between them. Secondly, a framework based on the machine learning algorithm is proposed to efficiently detect damage in rail head. Numerous inseparable guided wave modes are observed at higher frequencies implying the inability to detect damage through specific mode. Therefore, a machine learning framework is trained using time, frequency, and time–frequency domain features of the signal. Total 672 numerical simulations of different types of damage with different severity and location in the rail head are carried out to train and validate the model. It is found that GW generated through surface bonded PWTs is able to detect minimum defect size of 5% of head area with 1 mm thickness. Finally, the proposed framework is tested using simulation and experiment results of arbitrary damage in the rail head. The error in estimating severity was found to be in the range from 2.00% to 16.67%.

1. Introduction

Railways function as a lifeline to the country by transporting a considerable amount of total cargo and people from one place to another and by connecting remote locations. However, increasing cargo load, escalating train speed and low maintenance have increased train derailment risk. The direct and indirect cost of a rail accident is massive, and thus frequent monitoring of rail and timely maintenance is essential. The main cause for derailment is due to rail defects, especially in the head. Non-destructive testing (NDT) of the rail is done for regular monitoring and involves few methods such as visual inspections, ultrasonic testing, magnetic flux method and eddy current. Among these, ultrasonic testing is most prevalent and is done by examining the backscattering of incident ultrasonic wave from defect. However, due to limitation regarding test speed, the cascading effect of surface cracks and false damage detection, a faster and efficient method must be investigated.

Problems mentioned above with conventional ultrasonic testing on rail and benefits of guided wave (GW) in different domains of NDT such as plate, pipe, composites, embedded rebars and many more structures give rise to a research opportunity to use the guided wave for rail testing. Guided wave involves the multimodal transmission of an ultrasonic wave over long distance due to repeated reflection through a waveguide. Long-distance testing and damage sensitive modes help in determining both qualitative and quantitative nature of damage faster and more efficiently.

An initial study of the characteristics of guided wave in rail was done by Gavric (1995), through semi-analytical finite element method (SAFEM) for determining dispersion behaviour of rail for a frequency up to 6 kHz. Application of guided wave rail inspection was introduced by Rose, Avioli, and Song (2002), discussing ways for testing rail, which includes fixed sensors placed on the rail, rail inspection car with GW system and sensor placed on train. Application of finite element analysis and dispersive behaviour of rail was discussed by Sanderson and Smith (2000). Hayashi, Chiga, and Morimasa (2006) discussed wave structure for a rail for frequency less than 50 kHz and indicated the impracticality of perfect single-mode detection and excitation procedure. Non-contact transducer-based GW testing of rail was initially studied by McNamara and Lanza di Scalea (2002). Bartoli, Francesco, Mahmood, and Erasmo (2005) examined the waves in tens

* Corresponding author.
E-mail addresses: mahajanharsh1909@gmail.com (H. Mahajan), sauvik@civil.iitb.ac.in (S. Banerjee).
URL: https://www.civil.iitb.ac.in/~sauvik/ (S. Banerjee).

https://doi.org/10.1016/j.mlwa.2021.100216
Received 14 September 2021; Received in revised form 26 October 2021; Accepted 7 November 2021
Available online 20 November 2021

of kHz generated by impulsive excitation by using wavelet analysis and observed reflection from defect area up to 15% of the rail head area. Practical applications of non-contact sensing were illustrated by utilising laser and air-coupled transducers. The damage quantification was done by using a feature vector involving time and frequency parameters of signals. The features classified damages using Artificial neural network (di Scalea et al., 2005) and by performing outlier analysis (Rizzo et al., 2010). Coccia et al. (2011) provided insights into forced and unforced solutions of guided wave in rails using SAFEM and concluded the applicability of symmetric and non-symmetric load on rail head top to generate energy in top and side of the head. A full-fledged field experiment to check the efficiency of non-contact GW inspection of rail was conducted and presented (Mariani & di Scalea, 2018; Mariani et al., 2013). Authors concluded the effectiveness of system and challenges appeared due to acoustic impedance mismatch of air–steel interface.

Contact type GW has also been developed for a decade in order to continuous and long-range monitoring of the structure. It can overcome the challenges dealing with high noise in non-contact type of sensing as described above. Campos-Castellanos, Gharaibeh, P., and Kappatos (2011) had conducted the test to generate particular wave modes in head, web and foot through an arrangement of contact type transducers array. Although a little leakage of wave mode was found in all parts of rail, the study was concluded with the possibility of exciting mode that is specifically travelling in a portion of rail in lower frequency. Loveday (2008) had also investigated the behaviour of GW generated through contact type transducers through SAFEM simulation with a lower frequency of 12.5 kHz and concluded the study with good agreement between simulation and experiment results. Loveday and Long (2015) used laser vibrometer for the experiment and excited tone burst signal of 25 kHz and studied propagating modes.

Machine learning emerges as a new technique to link features of output data together and map it with damage severity, location, and classification. This technique gives results with good accuracy and can always be in the process of learning in order to improve prediction capability. Application of machine learning tools in health monitoring of various structural system has been increasing for a decade. It has been proved successful for investigating the damage in plates (Agarwal & Mitra, 2014; Ebrahimkhanlou, Brennan, & Salvatore, 2019; Hesser, Daniel, Georg, & Bernd, 2020; Karvelis, George, Vassilios, & Chrysostomos, 2020; Liu & Zhang, 2020; Rautela & Gopalakrishnan, 2021; Silva et al., 2020), pipelines (Diao et al., 2020; Sen et al., 2019), composites (Mardanshahi, Nasir, Kazemirad, & Shokrieh, 2020; Xu, Shenfang, Jian, & Yuanqiang, 2019), rails (Chen et al., 2018) etc. The main problem with the GW in rail is its numerous modes limiting the ability to investigate damage through mode-specific algorithms. Thus, machine learning can be utilised for determining damage in such cases.

From a review of past literature, it is found that previous attempts to utilise GW generated through surface bonded sensor for damage detection in rails is limited to generation of wave at lower frequency limiting its capability to detect small size damages. Therefore, in this study, we make an attempt to utilise high frequency GW signals in a relatively small rail specimen to determine damage type, damage severity and location zone of damage in rail head. A single contact type piezoelectric wafer transducer (PWT) attached to the web of the rail is used to generate GW, and its dispersion behaviour is studied using SAFE framework in COMSOL (COMSOL Multiphysics®, 2018). Due to multimodal nature of GW and inseparable modes at high frequencies, a machine learning framework to map damage features in rail head is developed and trained using features derived from time history, frequency spectrum and wavelet transform of the output signals Finally, the trained algorithm was tested for determining damage in simulations and experiments of artificial cracks of arbitrary sizes.

2. Guided wave in rail

Extensive experiments and simulations are conducted in an effort to understand the GW dispersion behaviour in rails generated by surface bonded PWT.

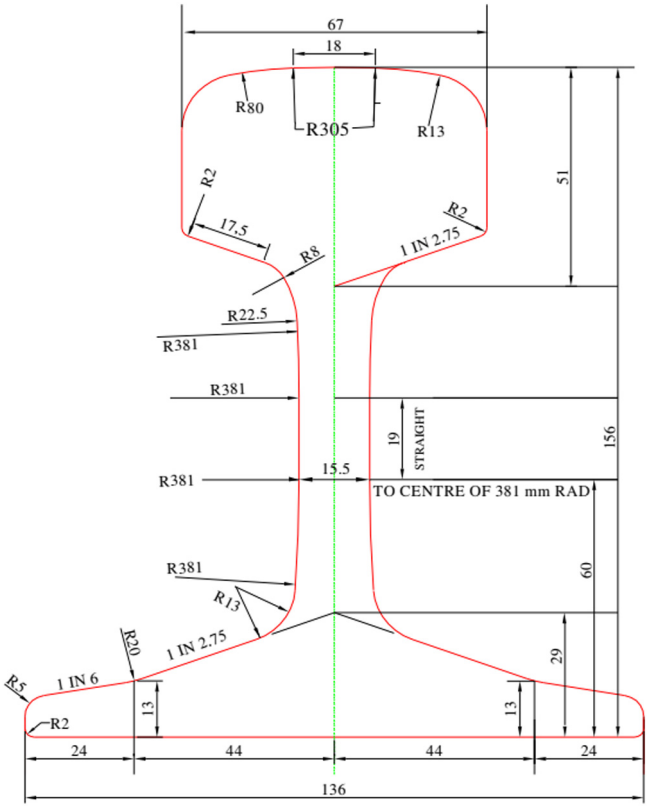

Fig. 1. Detail dimension of the cross-section of IRS 52 (RDSO Ministry of railways, 2009).

2.1. Experimental procedure

Tests are conducted in the laboratory on pristine rail section of IRS 52 having 1500 mm length with contact type PWTs. Fig. 1 represents the dimensions of rail.

The square type (20 mm × 20 mm × 0.3 mm) PWTs are attached to the rail web using a cyanoacrylate-based adhesive material to perform as transmitter and receiver in a pitch–catch arrangement. In field condition, the web is the accessible part of the rail where sensors can be attached. An input signal is generated using a function generator connected to an amplifier that sends an amplified signal to the transmitter. The transmitter is positioned at a distance of 100 mm from the receiver, which is connected to an oscilloscope for acquiring the resultant waveform (Fig. 2).

A Hanning window modulated five-cycle sine pulse is transmitted into the rail sample by using a function generator. The forcing function of the transmitted signal is given by Eq. (1)

$$f(t) = 0.5\left(1 - \cos\left(\frac{2\pi f_c t}{n}\right)\right) sin\left(2\pi f_c t\right) \quad (1)$$

where, f_c = Central frequency of the wave, n = number of cycles, t = time. The input signal at 120 kHz central frequency and its spectrum is shown in Figs. 3(a) and 3(b). To recognise the effectiveness of PWT at various central frequencies, the frequency modulation plot is generated by determining the peak amplitude of the received time-domain signal generated by an input pulse of a fixed central frequency. It is observed that PWT provides maximum responses at 45 kHz and 120 kHz as shown in Fig. 3(c). However, 120 kHz frequency is used for further study because higher frequency has a lesser wavelength, thus interacts well with smaller damages.

Artificial damage over the rail head is also provided. Transverse damage (TD) was created using grinder over the surface of the head. Two damage of approximate size of 17% and 38% head area are created

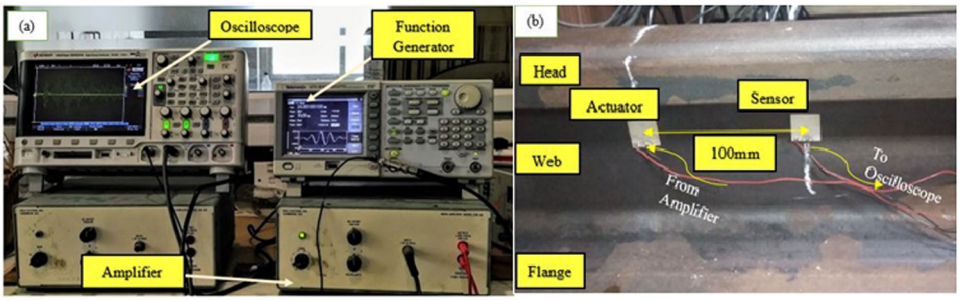

Fig. 2. Experimental setup: (a) Arrangement (b) Sensor position.

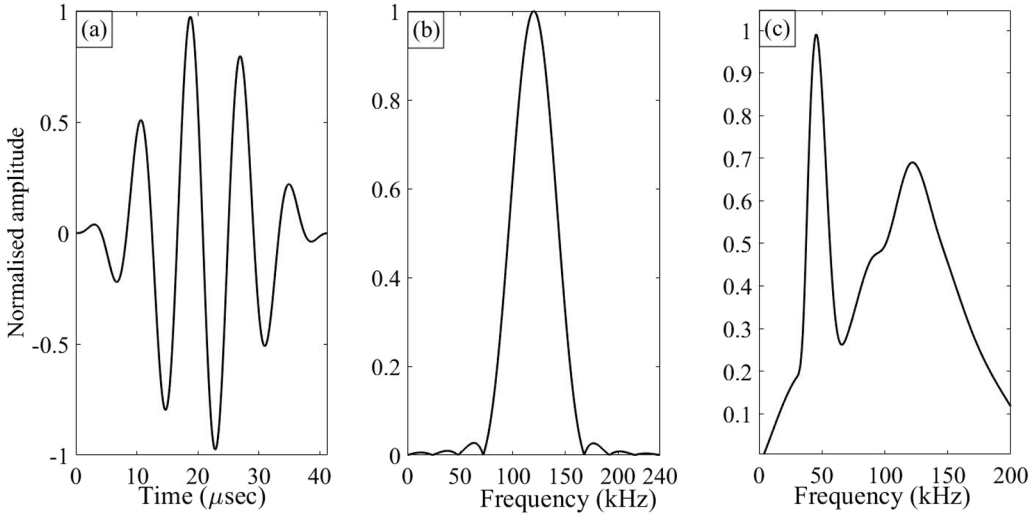

Fig. 3. (a) Input signal at 120 kHz (b) Spectrum of input signal (c) Frequency modulation curve for PWT-5H over the web of rail with a sensor placed at 100 mm centre to centre from actuator.

to test model. Fig. 4 shows pictures of TD in the rail head and the corresponding schematics to calculate damage area using full form CAD software.

2.2. Dispersion curve for rail

Determination of dispersion curve of an complex cross-section such as rail can be done using SAFEM (Gavric, 1995; Hayashi et al., 2006). In this method, the solution for the displacement field u can be proposed as simple harmonic vibration along the propagation direction.

$$u_i = U(y,z)e^{-i(kx-\omega t)} \tag{2}$$

where, k represents wavenumber, $\omega = 2\pi f$, f is the frequency, $i = \sqrt{-1}$, U represents the displacement amplitude in transverse direction. Hence, for SAFEM, only cross-section of waveguide need to be discretised.

Let us consider the displacement equation of motion

$$C_{ijkl}\frac{\partial^2 u_k}{\partial x_l \partial x_j} - \rho\frac{\partial^2 u_i}{\partial t^2} = 0 \tag{3}$$

where C_{ijkl} are the elastic constants and ρ is the density of the material. Substituting the value of u_i from Eq. (2) to Eq. (3), dividing equation with $e^{-i(kx-\omega t)}$ and appropriately renaming the dummy indices resulting in Eq. (4)

$$C_{ijkl}\frac{\partial^2 u_k}{\partial x_l \partial x_j} + ikC_{i3kl}\frac{\partial u_k}{\partial x_l} + ikC_{ijk3}\frac{\partial u_k}{\partial xj} - k^2 C_{i3k3}u_k + \rho\omega^2 u_i = 0; i,j,k,l \in \{1,2,3\} j,l \in \{1,2\} \tag{4}$$

The displacement of a particle can be deduced by displacement of the nodes and shape function. The strain and stress vectors of the element can also be expressed by the displacement of the nodes. According to the Hamilton principle, the dynamic equation of GW can be obtained

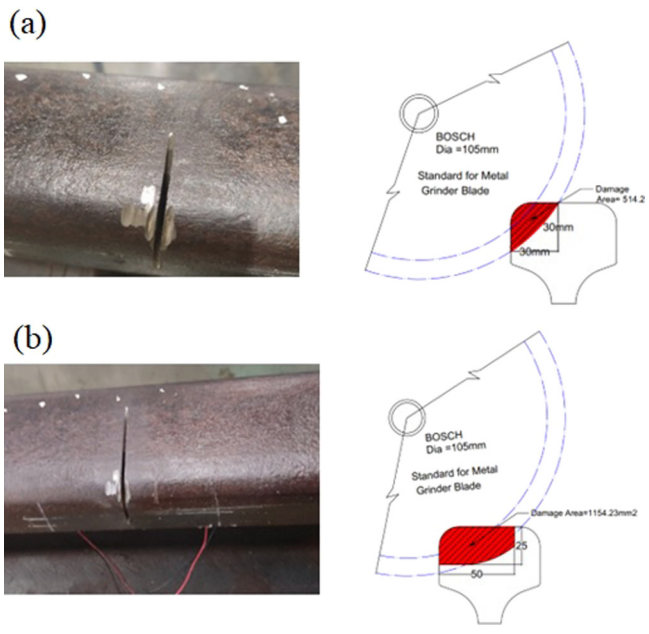

Fig. 4. Transverse damage in rail head at 50 mm from the actuator (a) 17% head area damage and schematics, (b) 38% head area damage and schematics.

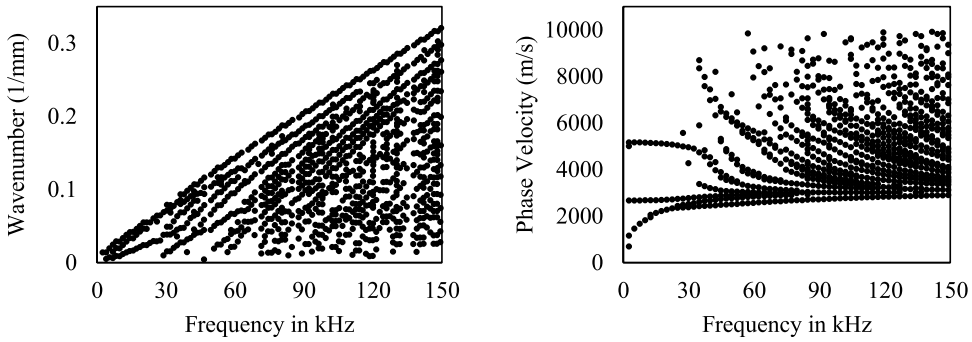

Fig. 5. Dispersion curve for rail section (a) wavenumber vs frequency (b) phase velocity vs frequency.

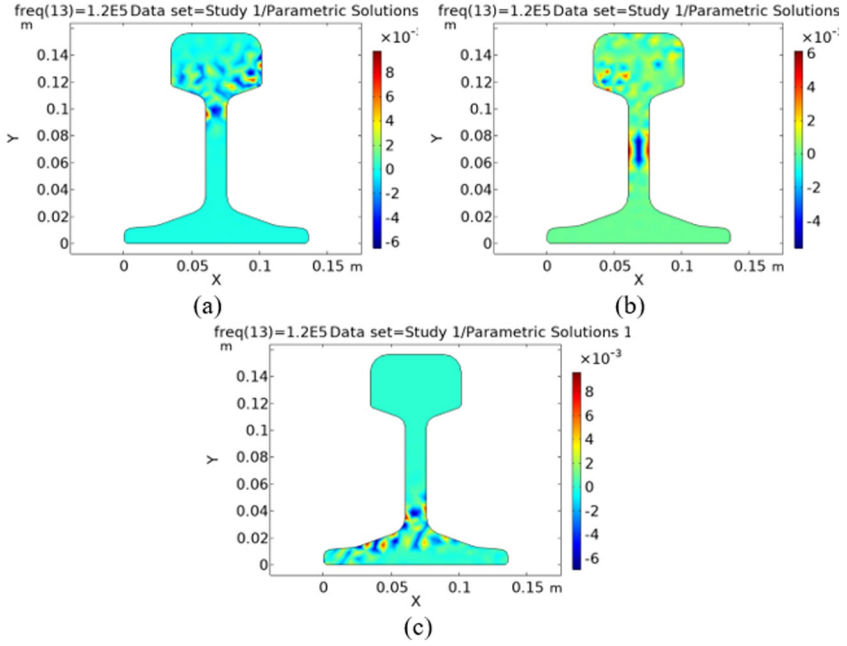

Fig. 6. Wave structure at a different wavenumber for frequency 120 kHz showing that energy is concentrated predominantly in (a) head (b) web and (c) flange.

by calculating strain energy and potential energy at any point simultaneously. Substituting strain and stress vectors in Hamilton formulation can be reduced to the following expression. (Eq. (5))

$$[K_1 + ikK_2 + k^2K_3 - \omega^2 M]U = 0 \tag{5}$$

From the above expression, an Eigen solution may be found by proposing a real positive ω and solving for the wavenumber k, as well as proposing a real or complex wavenumber and solving for the angular frequency ω. (Predoi, Michel, Bernard, & Christophe, 2007) deduced the above solution into generalised form of the differential equation that can be solved in a commercial FEM package that has the ability to solve generalised eigenvalue problems. COMSOL PDE interface (COMSOL Multiphysics®, 2018) has been used to solve the eigenvalue problem to generate a dispersion curve for rail.

SAFEM results in dispersion curve (Fig. 5), implying that numerous modes are present at higher frequencies. These modes travel at velocities remarkably close to each other. Unlike in plate, the modes of complex geometry are difficult to separate, analyse and utilise for damage detection. Fig. 6 also suggests that the presence of the energy of wave may be prevalent in one part but will also travel through all three parts of rail at a particular value of wavenumber.

2.3. Simulation of guided wave and its interaction with damage in rail

Analytical solution of wave propagation in a rail section is impractical due to its complex geometry involving multiple reflections. A finite element numerical simulation has been carried out in ABAQUS/6.14 (Abaqus, 2014) to analyse the guided wave propagation in the rail section. In the model, both explicit and implicit analysis is applied for dynamic simulation because only implicit analysis is not adequate for guided wave propagation, and the piezo-electric element is not present in the explicit part. Hence, rail was modelled as dynamic explicit, while the piezo-electric component is modelled as a dynamic implicit, and ABAQUS co-simulation technique is utilised to connect explicit and implicit parts. In the explicit part, ABAQUS C3D8R elements are used. Element size and time step are determined as per Courant–Friedrichs–Lewy (CFL) condition which states:

$$C = \frac{u\Delta t}{\Delta x} \leq C_{max} \tag{6}$$

where, u is the magnitude of velocity, Δt is the time step, Δx is the element size, C is Courant number

For a time-marching solver $C_{max} = 1$, hence

$$\begin{aligned} \frac{u\Delta t}{\Delta x} &\leq 1 \\ \frac{\Delta t}{\Delta x} &\leq \frac{1}{u} \\ \frac{\Delta t}{\Delta x} &\leq \frac{1}{\sqrt{v_L^2 + v_T^2}} \end{aligned} \tag{7}$$

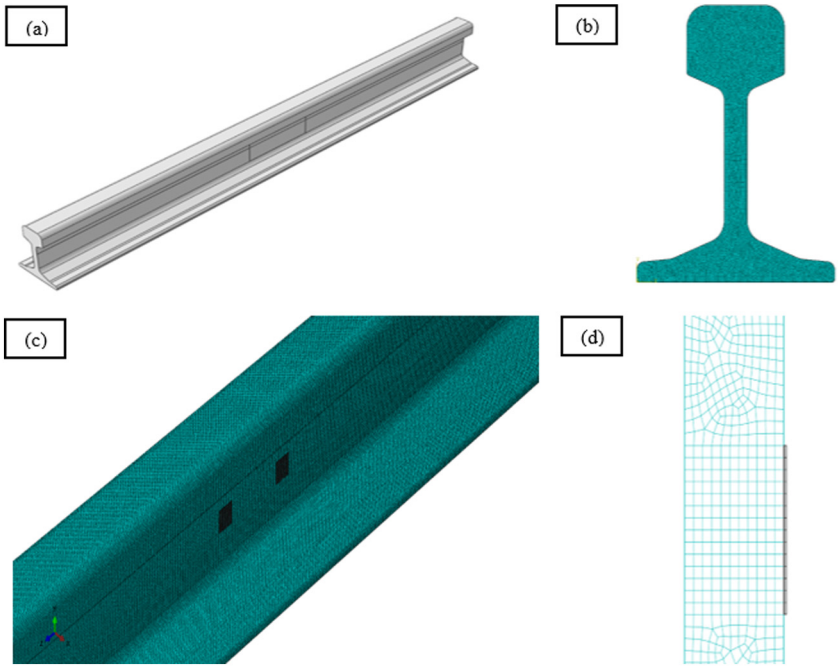

Fig. 7. Numerical simulation detail: (a) rail geometry (b) discretisation at rail cross-section (c) PWT on web and its meshing (3D view) (d) close-up of the cross-section of the web with PWT.

Optimum number of element per wavelength should be in between 10 to 40. Keeping 1 mm mesh size results optimum range of elements per wavelength for frequency up to 200 kHz.

For steel, V_L = 5778 m/s and V_T = 3142 m/s, on solving CFL condition

$$\Delta t \leq \frac{\Delta x}{\sqrt{v_L^2 + v_T^2}} = \frac{0.001}{6577.03} = 1.52e-7\,\text{s}$$

Where, V_L and V_T are the longitudinal and shear wave velocity, respectively. Time step need to be kept less than abovementioned value. Time step of 5e-8 s in ABAQUS solver results in complete analysis.

The PWTs are modelled as an assemblage of an electrode and a piezo element, both of size 20 mm × 20 mm connected through tie constraint. The electrode part is modelled as a homogeneous isotropic solid having mass density = 8700 kg/m^3, Young's modulus = 110 GPa, Poisson's ratio = 0.33 and thickness =0.1 mm. The meshing of the electrode is considered to be 1 mm and 8-noded linear brick element standard C3D8R is used as finite elements. The piezo element is modelled as a homogeneous anisotropic material of density 7750 kg/m^3 and having a damping (β) value of 0.000833. Standard C3D8E linear piezo-electric brick element is chosen for piezo-electric part, which is able to provide electromechanical coupling.

The other material properties are:

[ε] = piezo-electric permittivity matrix

$$\begin{bmatrix} 1.505 & 0 & 0 \\ 0 & 1.505 & 0 \\ 0 & 0 & 1.302 \end{bmatrix} \times 10^{-8}\,(\text{CV}^{-1}\text{m}^{-1})$$

[e] = piezoelectric stress matrix

$$\begin{bmatrix} 0 & 0 & 0 & 0 & 17 & 0 \\ 0 & 0 & 0 & 0 & 17 & 0 \\ -7.7 & -7.7 & 31.80 & 0 & 0 & \end{bmatrix} \times 10^3\,\text{N/m/V}$$

[c] = mechanical stiffness matrix

$$\begin{bmatrix} 12.6 & 7.95 & 8.41 & 0 & 0 & 0 \\ 0 & 12.6 & 8.41 & 0 & 0 & 0 \\ 0 & 0 & 11.7 & 0 & 0 & 0 \\ 0 & 0 & 0 & 2.3 & 0 & 0 \\ 0 & 0 & 0 & 0 & 2.3 & 0 \\ 0 & 0 & 0 & 0 & 0 & 2.35 \end{bmatrix} \times 10^{10}\,\text{Pa}$$

120 kHz input signal is applied to the top of transmitter piezo-electric element. Details of numerical simulation are provided in Fig. 7.

To recognise the change in signal due to damage, three types of damages originated in the head have been modelled that includes transverse damage (TD), horizontal split head (HSH) and vertical split head (VSH). TD is modelled as a circle inside the head with a thickness of one element, i.e., 1 mm, due to the resemblance of fracture growth in a circular manner (refer Fig. 8). The vertical split usually starts few millimetres below the surface of the rail. For the modelling, a gap of one element size, i.e., 1 mm is considered at the centre of cross-section of head and 5 mm below its top surface. Height of split is kept as 30 mm while the length is kept as a variable (Refer Fig. 9). Horizontal split is also modelled as damage with a thickness of one element, i.e., 1 mm. It is similar to vertical split but in the plane perpendicular to vertical split. Depth of split from the top is kept as 15 mm while the starting point's location, width, and length are kept variable (refer Fig. 10).

.

2.4. Validation of simulation model and analysis of GW propagation

A combined simulation and experimental study has been carried out to understand the applicability of PWTs over the rail for GW propagation. Input Signal of 120 kHz is actuated in simulation and experiment. The normalisation of signals needs to be done for correct interpretation of signals. Normalisation can be done with respect to maximum and minimum value of signal to scale it in specified range [−1, +1]. Fig. 11 shows the comparison between simulation and experimental data through time history plot, fast Fourier transform, and

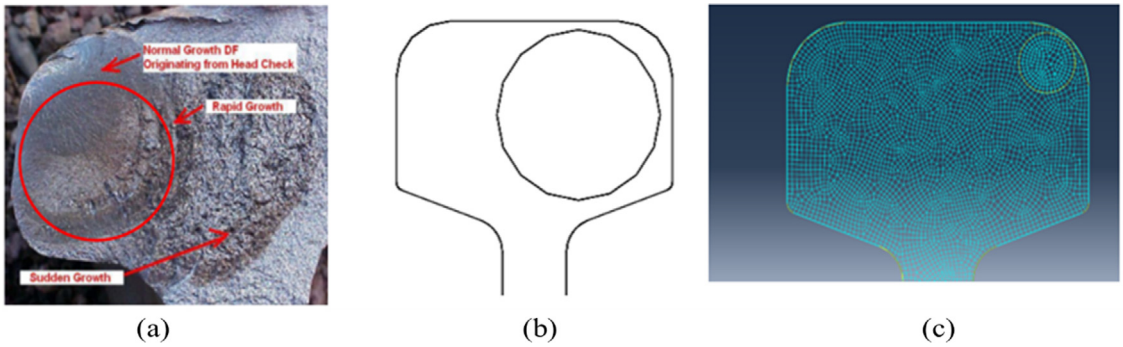

Fig. 8. Modelling of transverse damage in rail head. (a) Image of actual damage (b) Geometry (c) Discretisation.

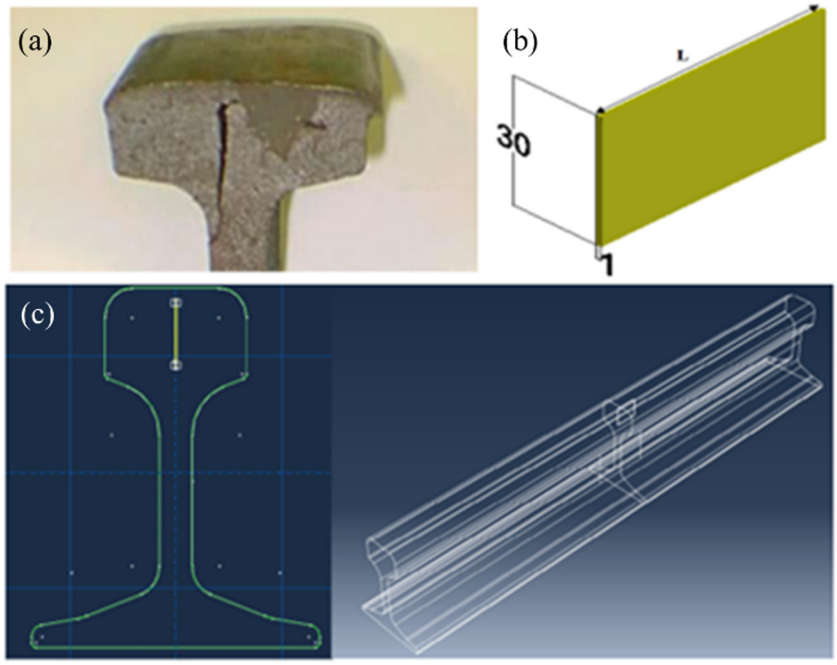

Fig. 9. Modelling of vertical split head in rail head. (a) Image of actual damage (b) Geometry (c) Location of damage.

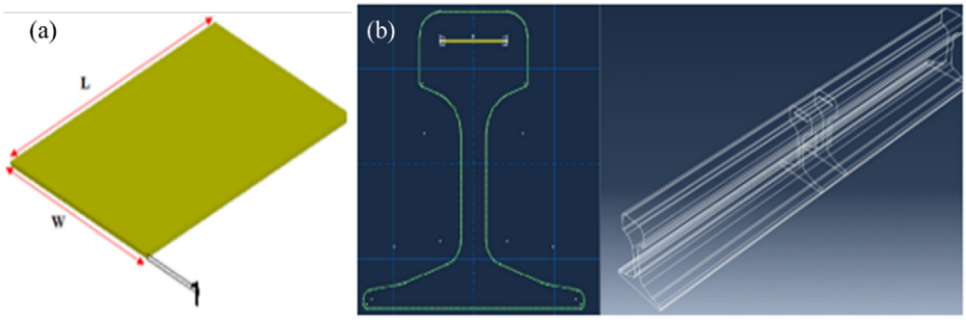

Fig. 10. Modelling of vertical split head in rail head. (a) Geometry (b) Location of damage.

wavelet transform. A great level of similarity between outputs can be observed. However, some phase mismatch may occur in both signals as damping factor has not been considered in the simulation.

Fig. 12a represents the change in signal due to TD of 17% head area located at a distance 50 mm from the actuator with respect to the experimental baseline signal. Similar behaviour can also be observed in the simulation resulting from 15% Head area damage (refer Fig. 12b). It can be observed that the starting portion of the signal is unaltered due to damage in both experiment and simulation.

The spherical waveform is generated from PWT actuator and interacted with boundaries of the rail section. These waves can be observed in Fig. 13 (left image) where displacements are shown as colour from blue to red depending on their magnitude, where blue being lower bound and red displays higher displacement. Fig. 13 (right image) shows the deformed shape of rail at various time instant. From both images, it can be noted that wave travel predominantly through the web in the initial time period ($t < 60$ μs), and afterwards, it travels through head and flange. The waveform and the deformed shape seems

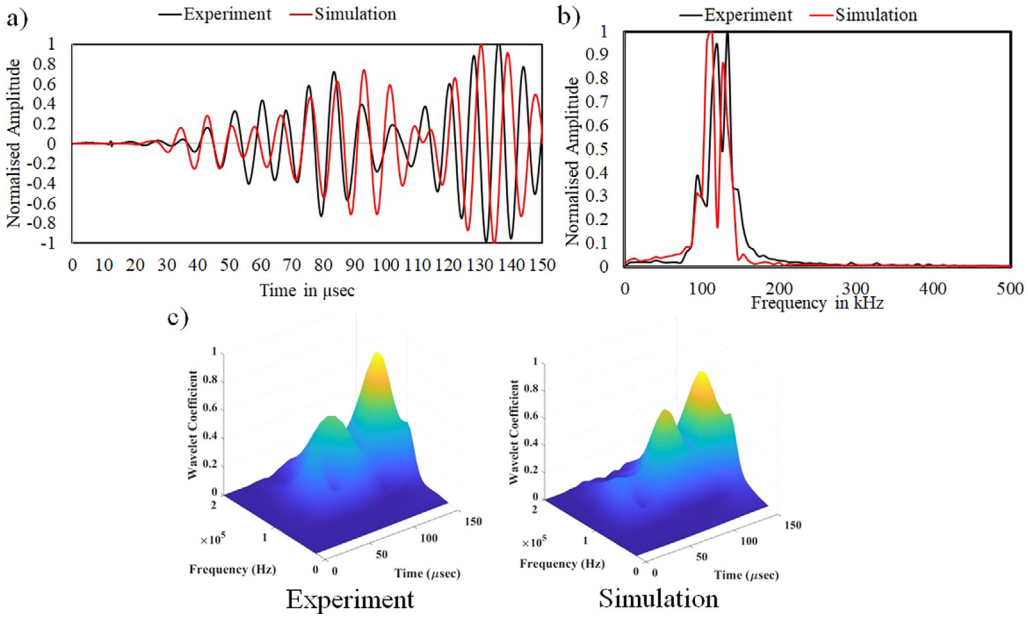

Fig. 11. Comparison of (a) time history plot (b) fast Fourier transform, and (c) wavelet transform between experiment and simulation results on pristine rail for exciting frequency of 120 kHz.

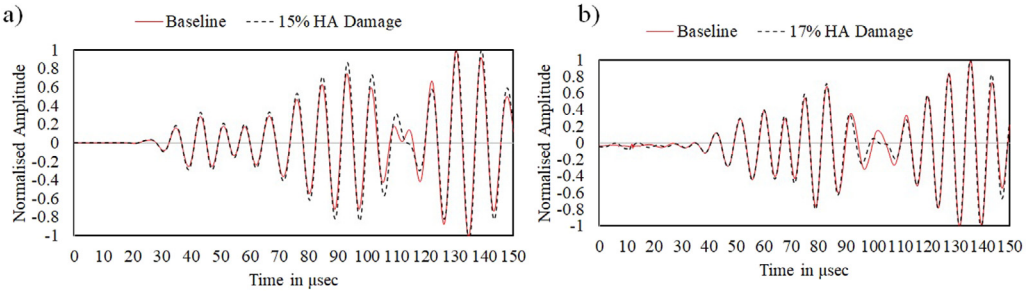

Fig. 12. Comparison between baseline and transverse damage in (a) experimental and (b) simulation results.

symmetrical around the actuator because the PZT actuator is located at the centre of the web and generates in plane wave motion in all directions.

3. Algorithm for damage detection

Dispersion behaviour and effect of damage in output signals as discussed in Section 2 suggest that damage in any part of rail viz. head, web, flange will affect the entire waveform. This leads to the inability to create a simple algorithm for damage detection. In such a case, machine learning algorithm is of great use as it can recognise the pattern change due to damage. In this section, a machine learning based algorithm has been developed, trained and tested with different damage datasets. A machine learning tool is very sophisticated in recognising the input parameter's pattern change and map it correctly with output results.

It is required to determine three parameters of the damage: type, location, and severity. A consolidated algorithm can be produced by proposing three loops for damage detection. The first loop will be the ML classifier algorithm for damage type. After the damage type is predicted, the next loop will be ML regression for estimation of damage size followed by a third loop to locate the damage zone through ML classifier (refer Fig. 14)

3.1. Machine learning algorithms

Proposed framework for identifying damage parameters can be separated as classification problem and regression problem. To determine damage type and zone, three supervised ML classification algorithms, namely K-nearest neighbours (KNN), decision tree (DT) and support vector machine (SVM) were taken into consideration. For estimation of damage severity, three supervised ML regression algorithms namely, linear regression, support vector regression and Gaussian process regression were used. Training results of considered algorithms are compared with each other.

KNN is a classifier based on the distance measurements of new data point from nearest k data points. The prediction of class of new data point is made based on majority class among the neighbour. A decision tree is essentially a hierarchy of condition statement of if/else trained through various features. A prediction can be made at a new data point by checking the region of the partition of feature space. SVM algorithm search a hyperplane in an n dimensional space (n-number of features) that distinctly classifies the data points. To create hyperplane, SVM chooses extreme points or vectors known as support vector. Linear SVM means dataset classified using a simple straight line. On the other hand, data in the real world may be non-linear and hence higher order polynomial can be used to define hyperplane. SVM may also be applied for a regression problem by setting a margin of tolerance to the support vectors. Linear regression establishes a linear relationship between input and output by minimising error using training data set. In Gaussian regression model, the Bayesian approach deduces a probability distribution over all possible values. Instead considering function between output and input, this approach works by specifying prior distribution on weight parameters. To get the prediction at a new point, a predictive distribution can be calculated by weighing all possible prediction by using prior and posterior distribution. The full

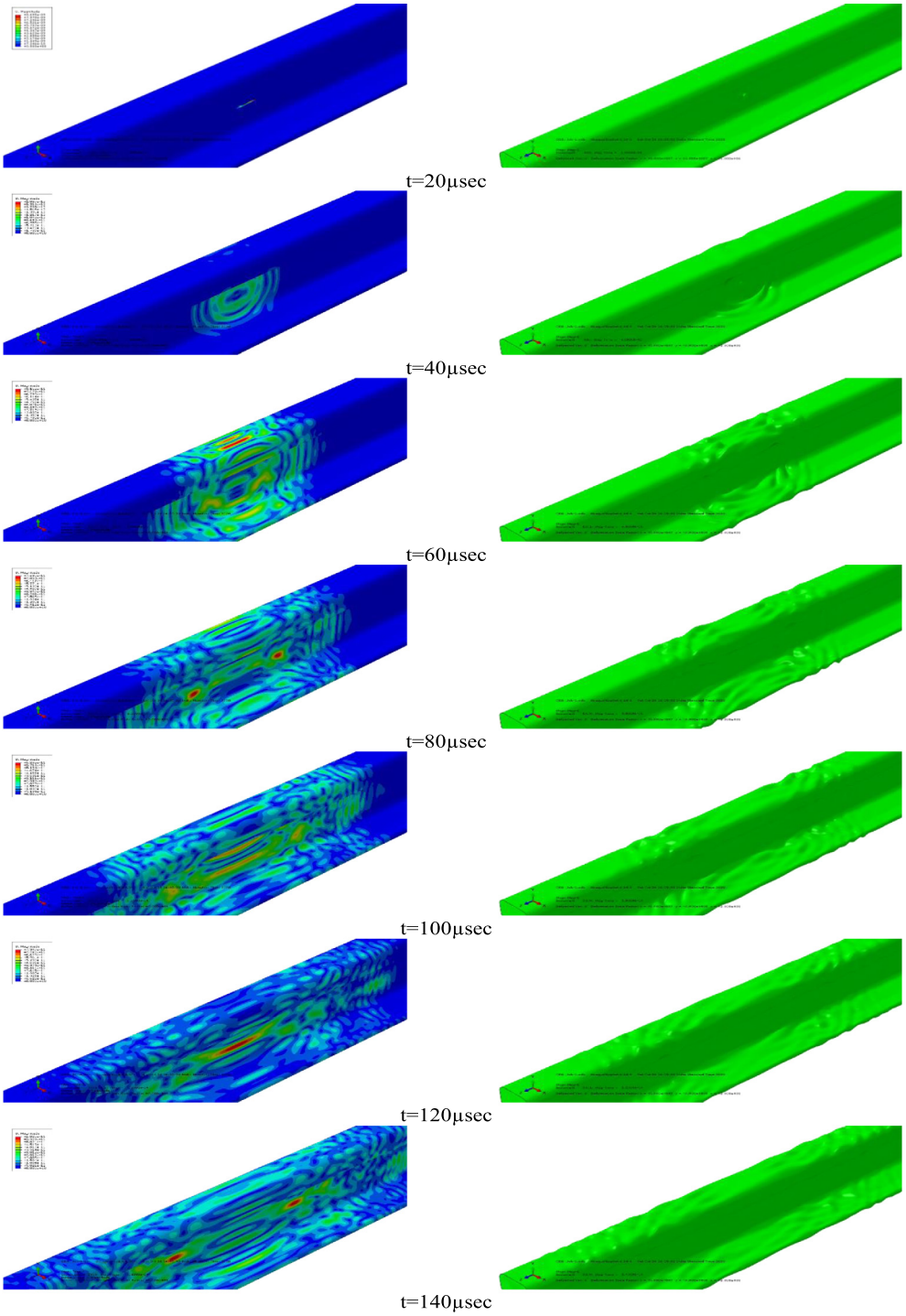

Fig. 13. Static images at different time values of the waveform (left image) and deformed shape (right image) of the rail due to generation of GW from actuator placed at the web.

description of working principles of considered ML algorithms is given in (Bishop, 2006; Géron Aurélien, 2019).

3.2. Feature extraction

Providing the whole signal as a feature vector for the ML algorithm is computationally inefficient practice and not necessarily provide all pattern information for prediction. Instead, a variety of parameters correlated with change in wave output due to the presence of damage can be developed as a feature vector for training and testing the ML algorithm.

Following are the features utilised to operate the ML-based prediction algorithm.

3.2.1. Peak to peak magnitude of signal:

It is the difference between maximum and minimum amplitude of a signal

$$Y_p = Y_{max} - Y_{min}$$

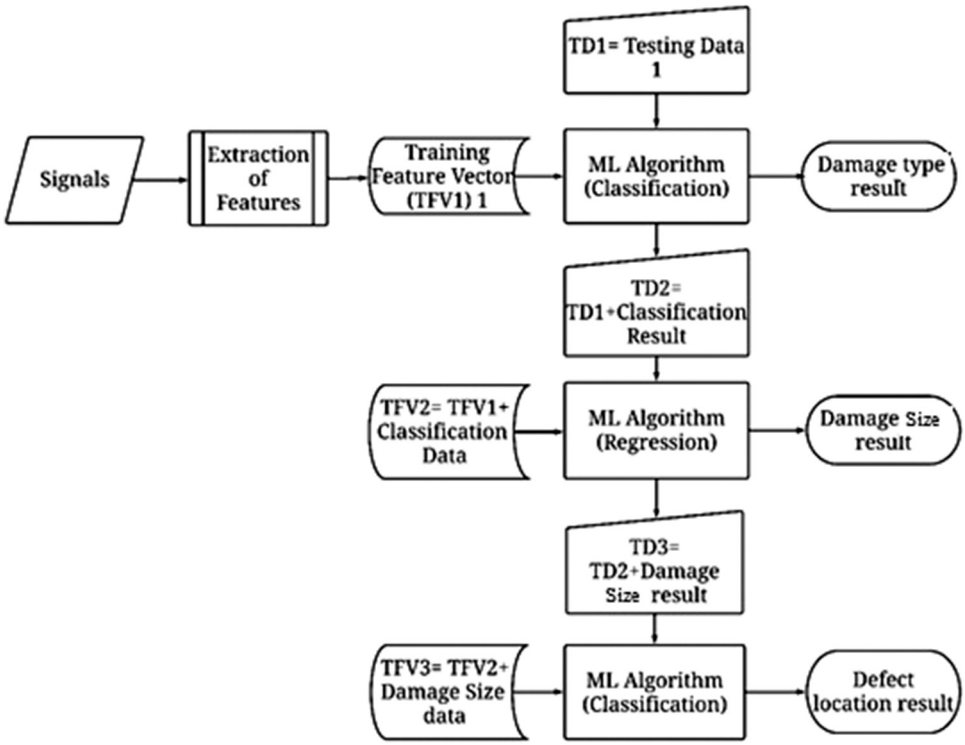

Fig. 14. Flow chart for the proposed framework for damage detection based on the machine learning algorithm.

3.2.2. Energy of signal

It is the Sum of the square of Signal amplitude

$$E = \sum_{n=1}^{N} Y^2(n)$$

3.2.3. Root mean square of signal

$$RMS = \sqrt{\frac{\sum_{n=1}^{N} Y(n)^2}{N}}$$

3.2.4. Fast Fourier transform:

FFT transforms signal from the time domain into the frequency domain. It calculates the discrete Fourier transform of the given signal using an FFT algorithm.

DFT is given by:

$$F(j\omega) = \sum_{k=0}^{N-1} f[k] e^{-j\omega kT}$$

The peak of FFT and area under FFT was taken as feature representing the frequency domain changes with respect to damage.

3.2.5. Wavelet coefficient at central frequency:

The wavelet transform of the signal represents the signal in frequency and time domain using the dilation and transition parameters. Continuous wavelets transform of the signal is done using analytical Morlet wavelet resulting in wavelet coefficients for a different time and pseudo-frequency. The value of the wavelet coefficient and its association with time and frequency is the essential feature of a signal.

The Equation of CWT is given by:

$$CWT(a,b) = \left(f, \psi_{a,b}\right) = \frac{1}{\sqrt{a}} \int_{-\infty}^{\infty} f(t)\, \psi^* \left(\frac{t-b}{a}\right) dt$$

In this work, the maximum coefficient of wavelet for central frequency (i.e. 120 kHz) is collected and maximum value of wavelet coefficient in three different time intervals: 0 to 100 μs (WTMax1); 100 μs to 150 μs (WTMax2) and 150 to 200 μs (WTMax3). Root mean square of wavelet coefficient (WTRMS) is also taken as a feature. Both peak and RMS value represent changes in the time–frequency domain.

All the extracted features are divided by respective values of baseline to compare the change in signal output due to damage. The algorithm is based on the relative change of features due to damage with respect to baseline. Hence, small mismatch in simulation and experimental signal may not affect the prediction to very large extent. To train the algorithm, damage severity is expressed as the percentage of rail head volume, i.e., area of rail head × length of the section to be inspected.

3.3. Training and testing data

As per the discussion in Section 2.2 and 2.3, the simulation results can be used for training the ML based framework for damage detection. Damage modelled in simulation and feature extracted from output result can generate a dataset for training and testing. Table 1 provides the detail of all damage models.

Here, Zone classifications have 5 zones viz. Zone1: 0 to 20 mm, Zone2: 21 to 40 mm, Zone3:41 to 60 mm, Zone4: 61 to 80 mm and Zone5: 81 to 100 mm. In practice, probability of additional noise in signal increases due to ambient noise, noise from electric system, weak bond between PWTs and surface etc. Therefore, white noise of amplitude varying from 2 to 10% of original signal was also added. There are total of 5 signals with noise level viz. 2%, 4%, 6%, 8% and 10% for each model. Hence, a dataset of 672 signals has been created for training and testing of ML algorithms.

4. Results and discussions

The ML algorithm is trained using SciKit Learn which is a statistics and ML library for Python.

Table 1
Details of damage models for ML algorithm training and testing.

Zone		Damage type					No. of model
	Base line	TD		HSH		VSH	
		Distance of plane	Damage area	Width (mm)	Length (mm)	Length (mm)	
No damage	1	–		–	–	–	**1**
Zone1	–	10			10, 20	10, 20	**16**
Zone2	–	30			10, 20, 60, 70	10, 20, 30,40, 50, 60	**26**
Zone3	–	45, 60	5% to 50% of head area	20, 40	10, 40, 60, 80	10, 20, 30,40, 50, 60, 70, 80	**38**
Zone4	–	70			10, 20, 40	10, 20, 30, 40	**20**
Zone5	–	90			10	10	**13**
Number of models	**1**	**60**		**30**		**21**	**112**

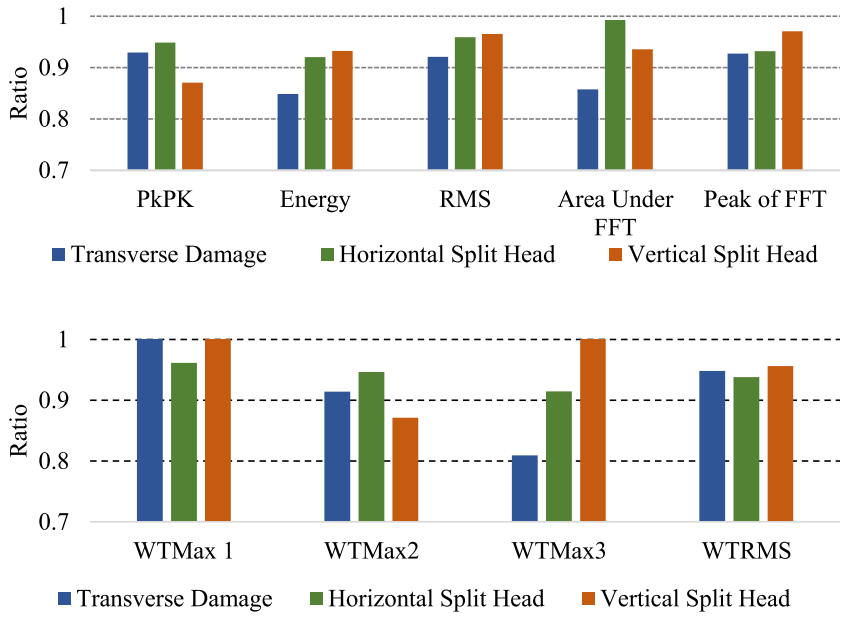

Fig. 15. Variation of features obtained from output signal due to presence of various type of damage in rail head of equivalent damage severity (~0.002%).

4.1. Feature variation

Three different types of damages were used to train and test the algorithm with varying severity and at various locations. Fig. 15 represents the variation of features with damage types for same damage severity. TD is present in a plane perpendicular to the propagating wave; hence it restricts more energy of wave. In contrast, VSH and HSH have lower interaction with the wave. Thus, by providing features variation, the algorithm can classify the damage type. In Fig. 16, for TD of 40% head area was analysed by observing the variation in the feature. It can be observed that the presence of damage in the various location have some effect but cannot establish similar trends for all zones.

Similarly, Fig. 17 represents the feature's variation with respect of damage extent for TD located at 45 mm from the actuator. A monotonic behaviour of the features can be observed, suggesting ML regression algorithm reliability based on provided features.

4.2. Training and testing results

Available dataset is divided into two parts: Training data and testing data with 70:30 ratios. Training data was utilised to train algorithm with 5-fold cross-validation. In-sample accuracy is then compared with out-of-sample accuracy by using testing data, to check against the overfitting. Random grid search was utilised for hyper-parameter optimisation. Table 2 enlist all and best parameters used for training.

Results of classification algorithms can be compared using metrics such as precision, recall, F1-score and AUC (Molin, Clifford, Rohan, & Ashok, 2021). Performance of regression algorithms can be done by comparing root mean square error (RMSE), mean absolute error (MAE) and mean square error (MSE) (Botchkarev, 2018).

Classification accuracy can be taken as performance scores to compare all optimised algorithms for classification respectively. In Fig. 18, comparison of training and validation scores are presented.

Tables 3 and 4 show the comparison of performance of classifiers for damage type and damage zone, respectively. For classification of damage type, SVM algorithm was observed to be best suitable while for zone classification, decision tree can be selected. While for regression problem of severity, Gaussian process regression can be identified as most accurate algorithm. (Refer Table 5)

The lower accuracy in zone classification is because the zone of HSH and VSH are classified based on the location of their centre point. However, due to their length, these damages are distributed in a large portion of rail head, while transverse damage is more reliable for classification of the zone of damage.

Finally, the prepared model is deployed and tested against simulation and experiment results of arbitrary chosen location and severity. From Table 6, it can be observed that the model predicts damage type with 100% accuracy, while the damage severity is predicted nearly to the actual value.

5. Conclusion

This study attempts to develop a GW-based method to detect rail head defects using a surface-bonded piezo wafer transducer. Generation of GW in rail presents a complex challenge to predict damage through

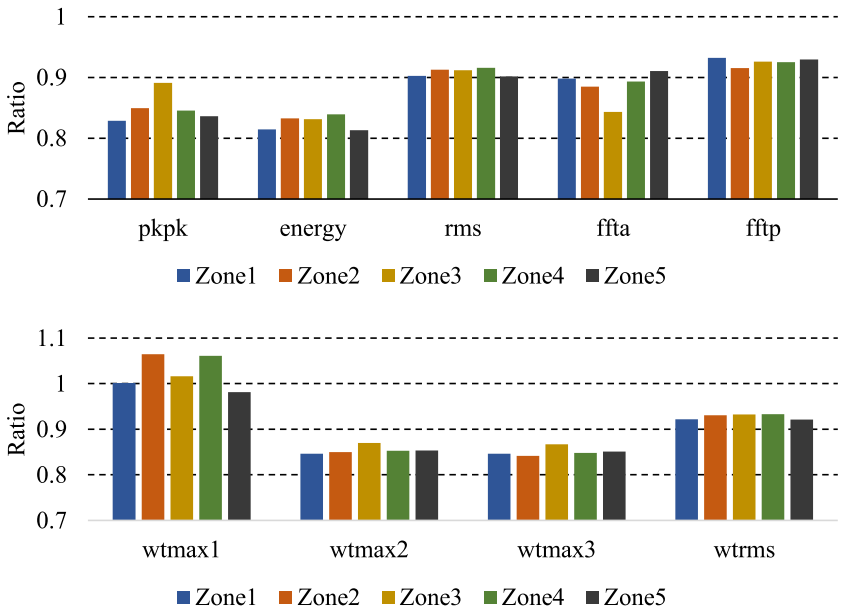

Fig. 16. Variation of features obtained from output signal due to presence of transverse damage of 40% head area damage located at various zone.

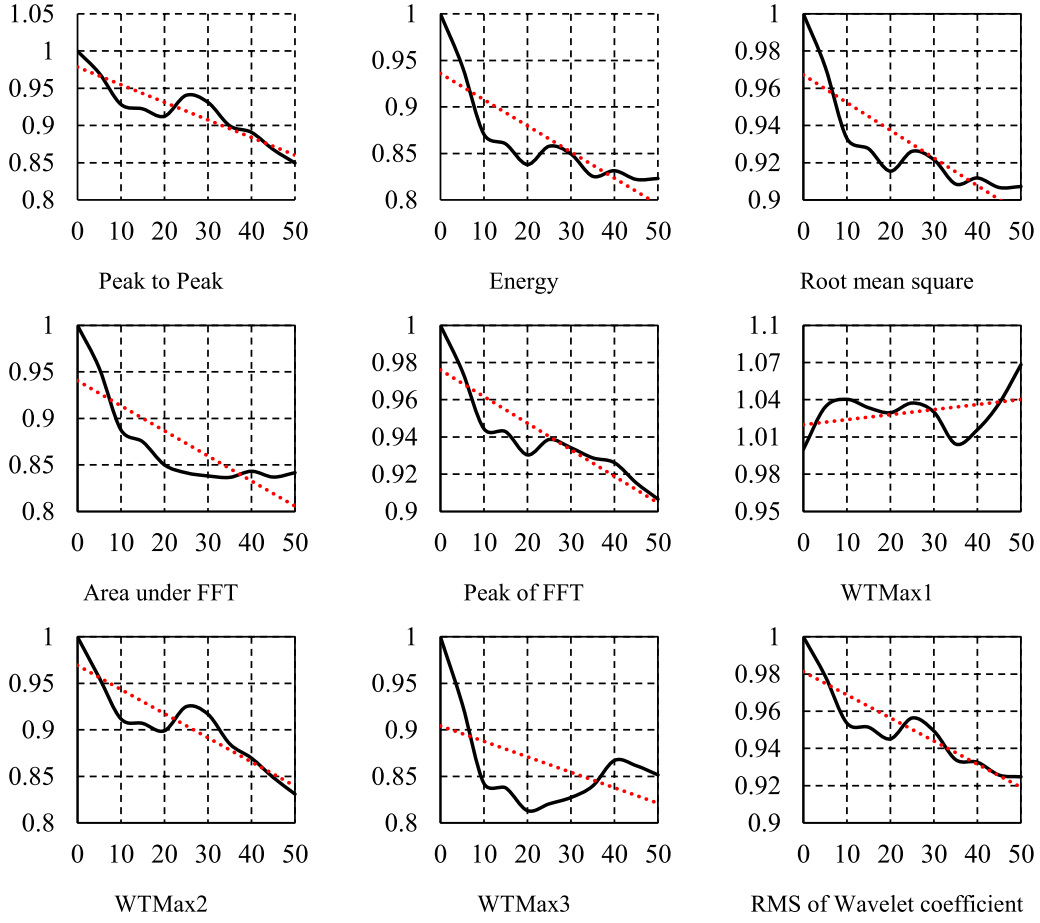

Fig. 17. Variation of features obtained from output signal due to presence of various damage severity of transverse damage located at 45 mm from actuator (x-axis: Damage area as % of Head area and y-axis: Features value).

an algorithm based on modal analysis. To cater to this problem, a predictive algorithm built on ML techniques is proposed, trained with resultant features of the simulated damage model's output signal. In the proposed framework, three different steps to predict three parameters of damage are used. For the classification of damage type, the SVM method is found to be highly accurate, whereas, for the regression analysis of damage severity Gaussian process regression is observed to be more precise. On the other hand, for zone classification, decision tree provides higher accuracy. The proposed framework is tested against the arbitrary damage located at different zones. For classification, the

Table 2
Selected algorithms with parameter variation.

Algorithm	Model	Parameters	Conditions	Optimum parameter	
				For type	For zone
Classifier	Decision Tree (DT)	Criterion	Gini, Entropy	Gini	Entropy
		Max Depth	$2n$, where $n = 1$ to 10	8	12
		Min sample leaf	2, 4, 6, 8	4	2
		Min sample split	5,10	10	2
	K nearest neighbour (KNN)	n neighbours	1 to 10	2	2
		Minkowski metric power parameter	1, 2	1	1
	Support vector machine (SVM)	C	0.01, 0.1, 1, 10, 100	0.01	100
		gamma	0.01, 0.1, 1, 10, 100	100	0.1
		Kernel	Linear, rbf, poly, sigmoid	Poly	Poly
		degree	2, 3, 4	3	4
Regression				For Severity	
	Ridge Linear Regression (RLR)	Alpha	0.0001 to 1000 in multiple of 10	0.001	
	Support vector regression (SVR)	Kernel	linear, rbf, poly	rbf	
		C	0.001, 0.01, 0.1, 1,10,100	0.001	
	Gaussian process regression (GPR)	Kernel	RBF, Matern, Rational quadratic, Exp-sine-squared	Exp-sine-squared	

Table 3
Performance metrics for type classification.

Algorithm	Class	Type				Macro average	Micro average
		No damage	TD	HSH	VSH		
SVM	Recall	**0.25**	**0.93**	**0.97**	**0.95**	**0.78**	**0.95**
	Precision	**1.00**	**0.87**	**0.97**	**0.95**	**0.95**	**0.95**
	F1 Score	**0.40**	**0.90**	**0.97**	**0.95**	**0.80**	
	AUC	**0.99**	**0.93**	**0.97**	**0.97**	**0.96**	
Decision Tree	Recall	0.50	0.84	0.97	0.92	0.81	0.93
	Precision	1.00	0.83	0.96	0.95	0.93	0.93
	F1 Score	0.67	0.84	0.96	0.93	0.85	
	AUC	1.00	0.89	0.96	0.96	0.95	
KNN	Recall	0.33	0.91	0.97	0.91	0.78	0.94
	Precision	1.00	0.89	0.98	0.86	0.93	0.94
	F1 Score	0.50	0.90	0.98	0.89	0.82	
	AUC	1.00	0.93	0.97	0.92	0.96	

Table 4
Performance metrics for zone classification.

Algorithm	Class	Zone					Macro average	Micro average
		1	**2**	**3**	**4**	**5**		
SVM	Recall	0.45	0.20	0.42	0.29	0.69	0.41	0.50
	Precision	0.73	0.02	0.85	0.12	0.35	0.42	0.50
	F1 Score	0.56	0.04	0.56	0.17	0.47	0.36	
	AUC	0.80	0.50	0.67	0.53	0.66	0.63	
Decision Tree	Recall	**0.50**	**0.73**	**0.77**	**0.47**	**0.75**	**0.64**	**0.50**
	Precision	**0.73**	**0.49**	**0.80**	**0.53**	**0.68**	**0.65**	**0.50**
	F1 Score	**0.59**	**0.59**	**0.78**	**0.50**	**0.71**	**0.63**	
	AUC	**0.81**	**0.72**	**0.85**	**0.70**	**0.82**	**0.78**	
KNN	Recall	0.37	0.35	0.65	0.35	0.90	0.53	0.50
	Precision	0.62	0.39	0.67	0.32	0.29	0.46	0.50
	F1 Score	0.46	0.37	0.66	0.34	0.44	0.45	
	AUC	0.73	0.58	0.76	0.60	0.64	0.66	

Table 5
Comparison between various machine learning regression model for prediction damage severity.

	Severity regression		
	RLR	SVM	GPR
Mean absolute error	0.000719	0.000749	**0.000333**
Mean square error	8.21×10^{-7}	1.66×10^{-6}	$\mathbf{2.35 \times 10^{-7}}$
Root mean square error	0.0091	0.0013	**0.0004**

model can predict the classification of damage with 100% accuracy for both simulation and experiment. The maximum error in predicting the damage is about 16.67% in case of VSH and minimum error is found to be 2.00% in case of TD for simulation results. This discrepancy in accuracy is due to the low number of training data for VSH and HSH compared to TD creating a bias in the model. For experimental results, the error is found to be approximately about 10%.

Current study is limited to head damage in a relatively small specimen with moderate accuracy in prediction using closely spaced PWTs. However, the proposed framework based on the ML algorithm could be used and trained with more rail damages and large PWT spacing requiring higher voltage requirements. The surface bonded PWT setup to detect damage in rail can be used as a real-time solution or can be attached to a rail car with linear array of sensor attached to arm which can come in contact with web, sensing a large section of rail at a time.

Table 6
Results from deployed model for experimental and simulation signals for arbitrary sized damage.

	True			Predicted			Error in %
	Damage type	Severity (as % of volume)	Zone	Damage type	Severity (as % of volume)	Zone	
Simulation	TD	0.0015	2 (35 mm)	TD	0.0017	2	13.33%
	TD	0.0035	2 (35 mm)	TD	0.0037	2	5.71%
	TD	0.0048	2 (35 mm)	TD	0.0046	2	4.17%
	TD	0.0012	3 (50 mm)	TD	0.0014	3	16.67%
	TD	0.0030	3 (50 mm)	TD	0.0026	3	13.33%
	TD	0.0050	3 (50 mm)	TD	0.0051	3	2.00%
	VSH	0.0037	2 (45 mm)	VSH	0.0040	4	8.11%
	VSH	0.0024	4(75 mm)	VSH	0.0028	4	16.67%
	HSH	0.0019	1 (17.5 mm)	HSH	0.0016	1	15.79%
	HSH	0.0021	3 (50 mm)	HSH	0.0023	4	9.52%
Experiment	TD	0.0017	3 (50 mm)	TD	0.0018	3	5.88%
	TD	0.0038	3 (50 mm)	TD	0.0042	4	10.53%

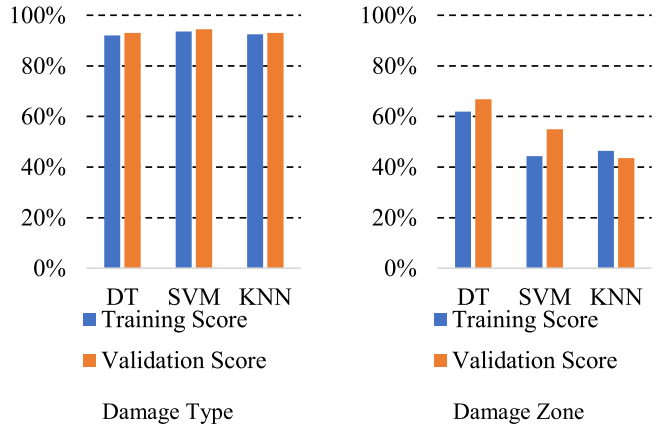

Fig. 18. Comparison of performance scores of various algorithms.

CRediT authorship contribution statement

Harsh Mahajan: Conceptualization, Data curation, Formal analysis, Investigation, Methodology, Software, Validation, Visualization, Writing - original draft. **Sauvik Banerjee:** Funding acquisition, Project administration, Resources, Supervision, Writing - review & editing.

Declaration of competing interest

The authors declare that they have no known competing financial interests or personal relationships that could have appeared to influence the work reported in this paper.

Acknowledgement

Authors want to acknowledge Jindal Steel & Power Limited for providing rail sections for experiments.

References

Abaqus 2014. User Mannual, Abaqus 6.14.

Agarwal, Sushant, & Mitra, Mira (2014). Lamb wave based automatic damage detection using matching pursuit and machine learning. *Smart Materials and Structures*, *23*(8).

Bartoli, Ivan, Francesco, Lanza Di Scalea, Mahmood, Fateh, & Erasmo, Viola (2005). Modeling guided wave propagation with application to the long-range defect detection in railroad tracks. *NDT and E International*, *38*(5), 325–334.

Bishop, Christopher M. (2006). Information science and statistics. In *Pattern recognition and machine learning*. Springer.

Botchkarev, Alexei (2018). Evaluating performance of regression machine learning models using multiple error metrics in azure machine learning studio. *SSRN Electronic Journal*.

Campos-Castellanos, C., Gharaibeh, Y., P., Mudge, & Kappatos, V. (2011). *The application of long range ultrasonic testing (LRUT) for examination of hard to access areas on railway tracks*. IET Conference Publications, 581 CP.

Chen, Wangcai, et al. (2018). Rail crack recognition based on adaptive weighting multi-classifier fusion decision. *Measurement: Journal of the International Measurement Confederation*, *123*(March), 102–114.

Coccia, Stefano, et al. (2011). Numerical and experimental study of guided waves for detection of defects in the rail head. *NDT and E International*, *44*(1), 93–100, http://dx.doi.org/10.1016/j.ndteint.2010.09.011.

COMSOL Multiphysics® (2018). *Reference manual, COMSOL 5.5*.

Diao, Xu, et al. (2020). Leak detection and location of flanged pipes: An integrated approach of principle component analysis and guided wave mode. *Safety Science*, *129*(March), Article 104809. http://dx.doi.org/10.1016/j.ssci.2020.104809.

Ebrahimkhanlou, Arvin, Brennan, Dubuc, & Salvatore, Salamone (2019). A generalizable deep learning framework for localizing and characterizing acoustic emission sources in riveted metallic panels. *Mechanical Systems and Signal Processing*, *130*, 248–272. http://dx.doi.org/10.1016/j.ymssp.2019.04.050.

Gavric, L. (1995). Computation of propagative waves. *Journal of Sound and Vibration*, *185*(3), 531–543.

Géron Aurélien (2019). *Hands-on machine learning with scikit-learn, keras, and tensorflow*. O'Reilly Media.

Hayashi, Takahiro, Chiga, Tamayama, & Morimasa, Murase (2006). Wave structure analysis of guided waves in a bar with an arbitrary cross-section. *Ultrasonics*, *44*(1), 17–24.

Hesser, Daniel, Frank, Georg, Karl Kocur, & Bernd, Markert (2020). Active source localization in wave guides based on machine learning. *Ultrasonics*, *106*.

Karvelis, Petros, George, Georgoulas, Vassilios, Kappatos, & Chrysostomos, Stylios (2020). Deep machine learning for structural health monitoring on ship hulls using acoustic emission method. *Ships and Offshore Structures*, 1–9. http://dx.doi.org/10.1080/17445302.2020.1735844.

Liu, Heng, & Zhang, Yunfen (2020). Deep learning based crack damage detection technique for thin plate structures using guided lamb wave signals. *Smart Materials and Structures*, *29*(1).

Loveday, Philip W. (2008). Simulation of piezoelectric excitation of guided waves using waveguide finite elements. *IEEE Transactions on Ultrasonics, Ferroelectrics and Frequency Control*, *55*(9), 2038–2045.

Loveday, Philip W., & Long, S. Craig (2015). Laser vibrometer measurement of guided wave modes in rail track. *Ultrasonics*, *57*(C), 209–217, http://dx.doi.org/10.1016/j.ultras.2014.11.010.

Mardanshahi, A., Nasir, S., Kazemirad, V., & Shokrieh, M. M. (2020). Detection and classification of matrix cracking in laminated composites using guided wave propagation and artificial neural networks. *Composite Structures*, *246*(April), Article 112403. http://dx.doi.org/10.1016/j.compstruct.2020.112403.

Mariani, Stefano, & di Scalea, Francesco Lanza (2018). Predictions of defect detection performance of air-coupled ultrasonic rail inspection system. *Structural Health Monitoring*, *17*(3), 684–705.

Mariani, Stefano, et al. (2013). Noncontact ultrasonic guided wave inspection of rails. *Structural Health Monitoring*, *12*(5–6), 539–548.

McNamara, John D., & Lanza di Scalea, Francesco (2002). Advances in health monitoring of railroad tracks. In *Smart nondestructive evaluation for health monitoring of structural and biological systems. Vol. 4702. No. 2002* (pp. 250–261).

Molin, Nicole L., Clifford, Molin, Rohan, J. Dalpatadu, & Ashok, K. Singh (2021). Prediction of obstructive sleep apnea using fast Fourier transform of overnight breath recordings. *Machine Learning with Applications*, *4*(2020), Article 100022. http://dx.doi.org/10.1016/j.mlwa.2021.100022.

Predoi, Mihai V., Michel, Castaings, Bernard, Hosten, & Christophe, Bacon (2007). Wave propagation along transversely periodic structures. *The Journal of the Acoustical Society of America*, *121*(4), 1935–1944.

Rautela, Mahindra, & Gopalakrishnan, S. (2021). Ultrasonic guided wave based structural damage detection and localization using model assisted convolutional and recurrent neural networks. *Expert Systems with Applications*, *167*(2020), Article 114189. http://dx.doi.org/10.1016/j.eswa.2020.114189.

RDSO Ministry of railways 2009. INDIAN RAILWAY STANDARD SPECIFICATION FOR FLAT BOTTOM RAILS (IRST-12-2009). Lucknow.

Rizzo, Piervincenzo, et al. (2010). Ultrasonic guided waves-based monitoring of rail head: Laboratory and field tests. In *Advances in civil engineering*.

Rose, J. L., Avioli, M. J., & Song, W. J. (2002). Application and potential of guided wave rail inspection. *Insight: Non-Destructive Testing and Condition Monitoring*, *44*(6), 353–358.

Sanderson, Ruth, & Smith, S. (2000). The application of finite element modelling to guided ultrasonic waves in rails. *Insight*, *44*(6), 359–363.

di Scalea, Francesco Lanza, et al. (2005). Non-contact ultrasonic inspection of rails and signal processing for automatic defect detection and classification. *Insight: Non-Destructive Testing and Condition Monitoring*, *47*(6), 346–353.

Sen, Debarshi, et al. (2019). Data-driven semi-supervised and supervised learning algorithms for health monitoring of pipes. *Mechanical Systems and Signal Processing*, *131*, 524–537. http://dx.doi.org/10.1016/j.ymssp.2019.06.003.

Silva, Lucas C., et al. (2020). Segmented analysis of time-of-flight diffraction ultrasound for flaw detection in welded steel plates using extreme learning machines. *Ultrasonics*, *102*(2019), Article 106057. http://dx.doi.org/10.1016/j.ultras.2019.106057.

Xu, Liang, Shenfang, Yuan, Jian, Chen, & Yuanqiang, Ren (2019). Guided wave-convolutional neural network based fatigue crack diagnosis of aircraft structures. *Sensors (Switzerland)*, *19*(16).